

A New Intensity-Hue-Saturation Fusion Approach to Image Fusion With a Tradeoff Parameter

Myungjin Choi, *Student Member, IEEE*

Abstract—A useful technique in various applications of remote sensing involves the fusion of panchromatic and multispectral satellite images. Recently, Tu *et al.* introduced a fast intensity-hue-saturation (IHS) fusion method. Aside from its fast computing capability for fusing images, this method can extend traditional three-order transformations to an arbitrary order. It can also quickly merge massive volumes of data by requiring only resampled multispectral data. However, fast IHS fusion also distorts color in the same way as fusion processes such as the IHS fusion technique. To overcome this problem, the minimization problem for a fast IHS method was considered and the method proposed by González-Audicana *et al.* is presented as a solution. However, the method is not efficient enough to quickly merge massive volumes of data from satellite images. The author therefore uses a tradeoff parameter in a new approach to image fusion based on fast IHS fusion. This approach enables fast, easy implementation. Furthermore, the tradeoff between the spatial and spectral resolution of the image to be fused can be easily controlled with the aid of the tradeoff parameter. Therefore, with an appropriate tradeoff parameter, the new approach provides a satisfactory result, both visually and quantitatively.

Index Terms—IKONOS image, image fusion, intensity-hue-saturation (IHS) method, Landsat Enhanced Thematic Mapper Plus (ETM+) image, multiresolution analysis, wavelet transform.

I. INTRODUCTION

THE FUSION of a panchromatic (Pan) image with a high spatial and low spectral resolution and multispectral (MS) images with a low spatial and high spectral resolution is an important issue in many remote sensing applications that require both high spatial and high spectral resolution, especially for GIS-based applications.

An image that has been well fused by an effective fusion technique is a useful tool not only for increasing the ability of humans to interpret the image but also for improving the accuracy of the classification [1]. In addition, a well-fused image gives a visually beautiful color image, especially for visualization purposes [2].

Many image fusion techniques and software tools have been developed for specific applications [3]–[17]. Of the hundreds of varied image fusion techniques, the best known methods are

the intensity-hue-saturation (IHS) technique, principal component analysis, arithmetic combinations, and wavelet-based fusion methods [2].

The IHS fusion technique, in particular, which is a popular image fusion method in the remote sensing community, has been used as a standard procedure in many commercial packages [18]. Recently, Tu *et al.* introduced a fast IHS fusion method [17]. Aside from its fast computing capability for fusing images, this method can extend traditional three-order transformations to an arbitrary order. It can also quickly merge massive volumes of data by requiring only resampled MS data. That is, it is well suited in terms of processing speed for merging new satellite images (such as IKONOS, QuickBird). However, fast IHS fusion also distorts color in the same way as fusion processes such as the IHS fusion technique. To reduce this spectral distortion, Tu *et al.* presented a simple spectral-adjusted scheme which they integrated into a fast IHS method.

In contrast, wavelet-based fusion methods, which are widely used as an image fusion technique, are based on multiresolution analysis. The wavelet approach preserves the spectral characteristics of the MS image better than the IHS method [8]. In general, however, images fused by wavelets have much less spatial information than those fused by the IHS method. Nonetheless, recent studies have shown that if an undecimated discrete wavelet transform (DWT) is used instead of the critically sampled DWT, the spatial resolution of the fused images can be as good as that of images obtained with the IHS fusion method [7]–[11]. An undecimated DWT, which is a shift-invariant form of the DWT, can be implemented by removing the down-sampling operations in the usual DWT implementation. It thereby avoids some of the artifacts that arise when the critically sampled DWT is used for image fusion [7]. Nevertheless, wavelet-based fusion methods are not efficient enough to quickly merge massive volumes of data from new satellite images because of its high computational complexity.

An advanced method of image fusion is needed; one that has fast computing capability, can reduce spectral distortion, and can preserve the high spatial quality. A new approach is therefore proposed, based on the fast IHS method. The new approach tries to minimize the spectral distortion inherent in image fusion methods that are based on IHS fusion. In the new approach, which is fast and convenient, the parameter t is used to appropriately control the tradeoff between the spatial and spectral resolution of the image to be fused. To validate the new approach, it was used to merge IKONOS images with Landsat Enhanced Thematic Mapper Plus (ETM+) Pan image and MS images. Then the spatial and spectral quality of the resulting

Manuscript received January 7, 2005; revised August 13, 2005. This work was supported in part by the Research Program of Satellite Technology Research Center, Korea Advanced Institute of Science and Technology.

The author is with Satellite Technology Research Center, Korea Advanced Institute of Science and Technology, Daejeon 305-701, Korea (e-mail: prime@satrec.kaist.ac.kr).

Digital Object Identifier 10.1109/TGRS.2006.869923

images were analyzed and compared to images obtained from wavelet-based fusion methods.

II. NEW APPROACH TO IMAGE FUSION

A. IHS Fusion Technique

The IHS fusion technique is widely used in image fusion to exploit the complementary nature of MS images [17]. The IHS fusion technique converts a color image from the red, green, and blue (RGB) space into the IHS color space. The intensity band (I) in the IHS space is replaced by a high-resolution Pan image and then transformed back into the original RGB space together with the previous hue band (H) and the saturation band (S), resulting in an IHS fused image. The IHS fusion for each pixel can be formulated by the following procedure.

Step 1)

$$\begin{bmatrix} I \\ v_1 \\ v_2 \end{bmatrix} = \begin{bmatrix} \frac{1}{3} & \frac{1}{3} & \frac{1}{3} \\ \frac{-\sqrt{2}}{6} & \frac{-\sqrt{2}}{6} & \frac{2\sqrt{2}}{6} \\ \frac{1}{\sqrt{2}} & \frac{-1}{\sqrt{2}} & 0 \end{bmatrix} \begin{bmatrix} R \\ G \\ B \end{bmatrix}. \quad (1)$$

Step 2) The intensity component I is replaced by the Pan image.

Step 3)

$$\begin{aligned} \begin{bmatrix} F(R) \\ F(G) \\ F(B) \end{bmatrix} &= \begin{bmatrix} 1 & \frac{-1}{\sqrt{2}} & \frac{1}{\sqrt{2}} \\ 1 & \frac{-1}{\sqrt{2}} & \frac{1}{\sqrt{2}} \\ 1 & \sqrt{2} & 0 \end{bmatrix} \begin{bmatrix} \text{Pan} \\ v_1 \\ v_2 \end{bmatrix} \\ &= \begin{bmatrix} 1 & \frac{-1}{\sqrt{2}} & \frac{1}{\sqrt{2}} \\ 1 & \frac{-1}{\sqrt{2}} & \frac{1}{\sqrt{2}} \\ 1 & \sqrt{2} & 0 \end{bmatrix} \begin{bmatrix} I + (\text{Pan} - I) \\ v_1 \\ v_2 \end{bmatrix} \\ &= \begin{bmatrix} R + (\text{Pan} - I) \\ G + (\text{Pan} - I) \\ B + (\text{Pan} - I) \end{bmatrix} \end{aligned} \quad (2)$$

where $F(X)$ is the fused image of the X band, for $X = R, G, B$, respectively.

Equation (2) states that the fused image $[F(R), F(G), F(B)]^T$ can be easily obtained from the original image $[R, G, B]^T$ simply by using addition operations. That is, the IHS method can be implemented efficiently by this procedure. This method is called the fast IHS fusion method [17].

The problem with the IHS method is that spectral distortion may occur during the merging process. In (2), the large difference between the values of Pan and I appears to cause the large spectral distortion of fused images. Indeed, this difference (Pan-I) causes the altered saturation component in the RGB-IHS conversion model [18].

B. Minimization Problem for the IHS Method

Next, let us consider the following minimization problem for the IHS method:

$$\min_{I_{\text{new}}} \{ |\text{Pan} - I_{\text{new}}|^2 + |I_{\text{new}} - I|^2 \} \quad (3)$$

where I_{new} is a gray-level image with a higher spatial resolution. First, although the term $\text{Pan} - I_{\text{new}}$ indicates that the spatial

resolution of the fusion result is higher than the original resolution whenever I_{new} is closer to Pan for each pixel, the spectral distortion of the fusion result is higher because the difference between I_{new} and I is larger. Second, although the term $I_{\text{new}} - I$ indicates that the spectral distortion of the fusion result is lower whenever I_{new} is closer to I for each pixel, the spatial resolution of the fusion result is lower than that of the result fused by the IHS method. As a result, depending on I_{new} , a tradeoff occurs between the spatial and spectral resolution of the fused image.

To solve the minimization problem, I_{new} may be closed to I in order to keep the spectral distortion low. In addition, I_{new} may simultaneously contain the Pan image's detailed information that is not present in the I image—this information is necessary for ensuring the high spatial resolution of the fused image. If necessary, an appropriate multiresolution transform can be used to extract the detailed spatial information of the Pan image.

C. Potential Solution for the Minimization Problem

Recently, the method introduced by González-Audicana *et al.* provides a solution for the minimization problem. In their method, multiresolution wavelet decomposition is used to execute the detailed extraction phase, and they follow the IHS procedure to inject the spatial detail of the Pan image into the MS image [7]. That is, I_{new} is the fusion result of the Pan and I images fused by a wavelet-based method of image fusion, which is expressed as follows:

$$I_{\text{new}} = I_r + \sum_{k=1}^n W_{P_k} \quad (4)$$

where I_r is the low-frequency version of the I image and $\sum_{k=1}^n W_{P_k}$ is the high-frequency version of the Pan image. Therefore, I_{new} contains the structural details of the Pan image's higher spatial resolution along with the rich spectral information of the MS images.

D. Potential Solution for the Spectral Distortion Problem

As mentioned, the spectral distortion problem arises from the change of saturation during the merging process. In an RGB-IHS conversion model, the saturation component (S) can be represented as follows:

$$S = 1 - \frac{3 \min\{R, G, B\}}{R + G + B} = \frac{I - X_0}{I} \quad (5)$$

where X_0 is the smallest value among R, G, and B [18].

Replacing the Pan value in (2) with the I_{new} value of (4) produces the following equation:

$$\begin{aligned} \begin{bmatrix} F(R) \\ F(G) \\ F(B) \end{bmatrix} &= \begin{bmatrix} R + (I_{\text{new}} - I) \\ G + (I_{\text{new}} - I) \\ B + (I_{\text{new}} - I) \end{bmatrix} \\ &= \begin{bmatrix} R + (I_r + \sum_{k=1}^n W_{P_k} - I) \\ G + (I_r + \sum_{k=1}^n W_{P_k} - I) \\ B + (I_r + \sum_{k=1}^n W_{P_k} - I) \end{bmatrix} \\ &= \begin{bmatrix} R + (\sum_{k=1}^n W_{P_k} - \sum_{k=1}^n W_{I_k}) \\ G + (\sum_{k=1}^n W_{P_k} - \sum_{k=1}^n W_{I_k}) \\ B + (\sum_{k=1}^n W_{P_k} - \sum_{k=1}^n W_{I_k}) \end{bmatrix} \end{aligned} \quad (6)$$

where $\sum_{k=1}^n W_{I_k}$ is the high-frequency version of the I image.

The new saturation value for the image fused by the method of González-Audícana *et al.* then becomes

$$\begin{aligned} S_{GA} &= 1 - \frac{3 \min\{R + \delta, G + \delta, B + \delta\}}{R + G + B + 3\delta} \\ &= 1 - \frac{X_0 + \delta}{I_{\text{new}}} = \frac{I - X_0}{I_{\text{new}}} \end{aligned} \quad (7)$$

where $\delta = I_{\text{new}} - I$.

The relation between (5) and (7) is

$$\frac{S_{GA}}{S} = \frac{\frac{I - X_0}{I_{\text{new}}}}{\frac{I - X_0}{I}} = \frac{I}{I_{\text{new}}} = \frac{I}{I + \delta}. \quad (8)$$

This δ parameter is therefore a crucial factor in the spectral distortion problem when the difference between the values of I_{new} and I is large. See [18] for more details.

In contrast, the saturation value of the image fused by the method of González-Audícana *et al.* is similar to that of the image fused by the wavelet substitution method introduced by Núñez *et al.* [13]. To prove this, we assumed that the wavelet substitution method used an undecimated wavelet transform for the multiresolution analysis. Consequently, we obtained the following fused result:

$$\begin{aligned} \begin{bmatrix} F(R) \\ F(G) \\ F(B) \end{bmatrix} &= \begin{bmatrix} R_r + \sum_{k=1}^n W_{P_k} \\ G_r + \sum_{k=1}^n W_{P_k} \\ B_r + \sum_{k=1}^n W_{P_k} \end{bmatrix} \\ &= \begin{bmatrix} R + \sum_{k=1}^n W_{P_k} - \sum_{k=1}^n W_{R_k} \\ G + \sum_{k=1}^n W_{P_k} - \sum_{k=1}^n W_{G_k} \\ B + \sum_{k=1}^n W_{P_k} - \sum_{k=1}^n W_{B_k} \end{bmatrix} \end{aligned} \quad (9)$$

where R_r , G_r , and B_r are the low-frequency version of R , G , and B , respectively, and $\sum_{k=1}^n W_{R_k}$, $\sum_{k=1}^n W_{G_k}$, and $\sum_{k=1}^n W_{B_k}$ are the high-frequency version of R , G , and B , respectively.

The subsequent result is

$$\begin{aligned} S_{GA} &= 1 - \frac{\sum_{k=1}^n W_{P_k} - X_0}{I + \sum_{k=1}^n W_{P_k} - \Delta X_0} \\ &\approx 1 - \frac{\sum_{k=1}^n W_{P_k} - X'_0}{I + \sum_{k=1}^n W_{P_k} - \Delta X'_0} \\ &= S_{WS} \end{aligned} \quad (10)$$

where $X_0 = \min\{R - \sum_{k=1}^n W_{I_k}, G - \sum_{k=1}^n W_{I_k}, B - \sum_{k=1}^n W_{I_k}\}$, $X'_0 = \min\{R - \sum_{k=1}^n W_{R_k}, G - \sum_{k=1}^n W_{G_k}, B - \sum_{k=1}^n W_{B_k}\}$, $\Delta X_0 = \sum_{k=1}^n W_{I_k}$, and $\Delta X'_0 = (\sum_{k=1}^n W_{R_k} + \sum_{k=1}^n W_{G_k} + \sum_{k=1}^n W_{B_k})/3$.

From (10), the spectral quality of the image fused by the method of González-Audícana *et al.* is similar to that of the image fused by the wavelet substitution method. Indeed, the experimental results shown in the next chapter support this fact. Moreover, whenever the method of González-Audícana *et al.* uses the fast IHS method instead of the IHS transform, its processing speed is quicker than the wavelet substitution method.

E. Reasons for the Inefficiency of Wavelet-Based Image Fusion

In general, most types of wavelet-based image fusion provide a fused image with low spatial resolution. Recently, some studies have shown that the use of a redundant DWT (such as an undecimated à trous wavelet transform [19]) produces a satisfactory spatial resolution [7]–[11]. This phenomenon occurs

because a redundant DWT can avoid some of the artifacts that arise when a critically sampled DWT is used for image fusion; for example, when there is a loss of linear continuity in the spatial details, such as in plot edges, railways, or roads [7]. Nevertheless, the wavelet-based fusion method is not efficient enough to quickly merge massive volumes of data from new satellite images because of its high computational complexity.

We therefore need to develop an advanced image fusion method that has a fast computing capability, can reduce spectral distortion, and can preserve the high spatial quality.

F. New Approach to Image Fusion

To solve the minimization problem for IHS fusion, we can simply calculate the second order equation, the solution of which is as follows: I_{new} is equal to $(\text{Pan} + I)/2$. Whenever I_{new} is closer to Pan for each pixel, the difference between I_{new} and I for each pixel is larger, and this difference causes a spectral distortion. Conversely, whenever I_{new} is closer to I for each pixel, the spatial resolution of the fusion result is lower. Therefore, $(\text{Pan} + I)/2$ is an appropriate linear solution for I_{new} .

Next, let us consider that $I_{\text{new}} = \text{Pan} - (\text{Pan} - I)/t$ when we use the parameter t . Then, for $t = 1$, I_{new} equals I , which is the same as before the fusion. That is, the fused image has no spectral distortion but may theoretically have the lowest spatial resolution. For $t = 2$, I_{new} is equal to $(\text{Pan} + I)/2$. If t increases to infinity, I_{new} equals Pan , as in the IHS fusion method. That is, the fused image has the largest spectral distortion but may have a high spatial resolution. In summary, as the corresponding t increases from 1 to infinity, the spatial resolution and the spectral distortion increase. This result means that the tradeoff between the spatial and spectral resolution of the image to be fused can be controlled by using parameter t , which is called the tradeoff parameter. The proposed method is expressed as follows:

$$\begin{aligned} \begin{bmatrix} F(R) \\ F(G) \\ F(B) \end{bmatrix} &= \begin{bmatrix} R + (I_{\text{new}} - I) \\ G + (I_{\text{new}} - I) \\ B + (I_{\text{new}} - I) \end{bmatrix} \\ &= \begin{bmatrix} \text{Pan} - \frac{(\text{Pan} - I)}{t} + (R - I) \\ \text{Pan} - \frac{(\text{Pan} - I)}{t} + (G - I) \\ \text{Pan} - \frac{(\text{Pan} - I)}{t} + (B - I) \end{bmatrix}. \end{aligned} \quad (11)$$

This method of image fusion is very fast and easy to implement because all the MS images can be fused at one time. If the original MS and Pan images are geo-referenced, the resampling process can be accomplished together with the fusion in one step. Moreover, according to the purpose of each application, different user-specified tradeoff parameters can be used for user-specified MS images.

G. IKONOS Image Fusion

When IHS-like fusion methods are used with IKONOS imagery, there is a significant color distortion, due primarily to the range of wavelengths in an IKONOS Pan image. Unlike the Pan images of SPOT and IRS sensors, IKONOS Pan images (as shown Fig. 1) have an extensive range of wavelengths—from visible to near-infrared (NIR). This difference obviously induces

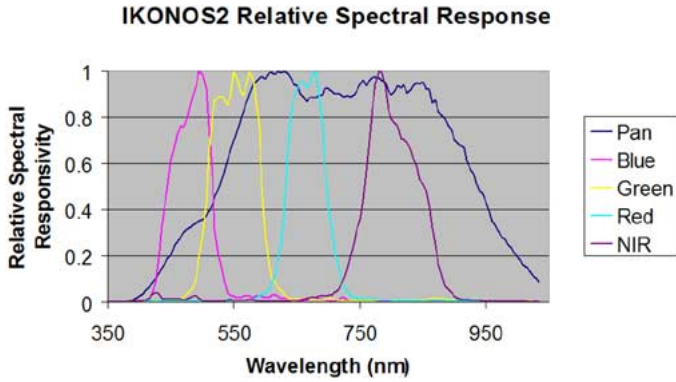


Fig. 1. IKONOS relative spectral responses.

the color distortion problem in IHS fusion as a result of the mismatches; that is, the Pan and I are spectrally dissimilar. In particular, the grey values of Pan in the green vegetated regions are far larger than the grey values of I because the areas covered by vegetation are characterized by a relatively high reflectance of NIR and Pan bands as well as a low reflectance in the RGB bands. To minimize the radiance differences between I and Pan, Tu *et al.* included the NIR band in the definition of the I component [17]. Indeed, the fusion algorithm proposed by Tu *et al.* reduces the color distortions in fused images, especially on vegetated areas. To include the response of the NIR band in I, the proposed method was extended from three to four bands, and expressed as follows:

$$\begin{bmatrix} F(R) \\ F(G) \\ F(B) \\ F(NIR) \end{bmatrix} = \begin{bmatrix} Pan - \frac{(Pan-I')}{t} + (R - I') \\ Pan - \frac{(Pan-I')}{t} + (G - I') \\ Pan - \frac{(Pan-I')}{t} + (B - I') \\ Pan - \frac{(Pan-I')}{t} + (NIR - I') \end{bmatrix} \quad (12)$$

where $I' = (R + G + B + NIR)/4$.

III. EXPERIMENTAL STUDY AND ANALYSIS

To merge IKONOS Pan and MS images, an image of the Korean city of Daejeon was used, which was acquired on March 9, 2002. The IKONOS imagery contains a 1-m Pan image and four-band 4-m MS images. The data for this experiment comprise a Pan image and four R, G, B, and NIR MS images.

To merge Landsat ETM+ Pan and MS images, an image, taken on April 3, 2002, was used, which was an L1G product of path 116 and row 34. The Landsat ETM+ image has eight bands with three different resolutions:

- 30 m for bands 1 to 5 and 7;
- 60 m for band 6;
- 15 m for band 8.

Band 8 was used as the Pan image. For the MS images, images converted to the RGB system were used, with the following transformation:

- $R = (B5 + B7)/2$;
- $G = (B3 + B4)/2$;
- $B = (B1 + B2)/2$.

A. Quantitative Analysis

The quantitative analysis is based on the experimental results for the factors used in [3]–[8], [20], [21]: namely, the bias, the standard deviation (SD), the correlation coefficient (CC), the relative average spectral error (RASE), the *erreur relative globale adimensionnelle de synthèse* (ERGAS), new image quality index $Q4$, image fusion performance measure (IFPM), and spatial quality measurement proposed by Zhou *et al.*

To assess the spectral and spatial quality of the fused images, spatially degraded Pan and MS images from the original images were used. For the experiment on the fusion of IKONOS images, the derived images have a resolution of 4 and 16 m, respectively. These images were synthesized at a 4-m resolution and then compared to the original IKONOS MS images. Using these eight factors, Tables I and III compare the experimental results of image fusion for the proposed method, the IHS method, and wavelet-based methods.

For the experiment on the fusion of the Landsat ETM+ images, the derived images have a resolution of 30 and 60 m, respectively. These images were similarly synthesized at a 30-m resolution and then compared to the original Landsat ETM+ MS images. Table II and IV compare the experimental results of the image fusion.

1) *Bias, the SD, and the CC*: The bias refers to the difference in radiance between the means of the original and fused images and the value of the difference relative to the mean of the original image. The smaller the difference, the better the spectral quality.

The SD of the difference image in relation to the mean of the original image indicates the level of the error at any pixel. The lower the value of this parameter, the better the spectral quality of the fused image.

The CC between the original and fused image is defined as

$$CC(A, B) = \frac{\sum_{m,n} (A_{mn} - \bar{A})(B_{mn} - \bar{B})}{\sqrt{(\sum_{m,n} (A_{mn} - \bar{A})^2) (\sum_{m,n} (B_{mn} - \bar{B})^2)}} \quad (13)$$

where \bar{A} and \bar{B} stand for the mean values of the corresponding data set, and CC is calculated globally for the entire image. The result of this equation shows similarity in the small structures between the original and fused images.

Tables I and II show the fusion results of the IHS method, the wavelet additive method (udWA), the wavelet substitution method (udWS), the method of González-Audicana *et al.* (udGA), the ARSIS concept with the RWM model (udRWM), and the proposed method with four different tradeoff parameters. Note that all wavelet-based methods use an undecimated à trous wavelet transform because some studies have shown that this redundant wavelet transform is more suitable than the standard orthogonal wavelet transform for multisensor image fusion [7]–[11].

Table I shows that with our proposed method the values of the bias and SD monotonically increase when t increases from 2.0 to 5.0, whereas the CC decreases. This result means that the spectral distortion increases, corresponding to t enlarges, in images fused by the proposed method. In Table II, the pattern of the values of the bias, SD, and CC of the proposed method has global similarity with the values of Table I.

TABLE I
IKONOS IMAGE FUSION RESULTS

		Initial	$t = 2.0$	$t = 3.0$	$t = 4.0$	$t = 5.0$	IHS	udWA	udWS	udGA	udRWM
Bias(%) (ideal value:0)	R	0.000	0.913	1.218	1.370	1.461	1.827	0.990	0.699	0.696	0.039
	G	0.000	1.025	1.367	1.539	1.641	2.052	1.113	0.882	0.782	0.063
	B	0.000	1.076	1.435	1.615	1.723	2.154	1.168	0.943	0.822	0.060
SD(%) (ideal value:0)	R	25.71	19.19	19.46	19.81	20.15	22.34	19.96	18.80	17.83	21.26
	G	26.51	20.57	20.98	21.66	22.21	25.28	22.95	21.37	20.20	22.57
	B	24.95	20.89	22.26	23.40	24.22	28.21	26.93	25.50	23.51	23.40
CC (ideal value:1)	R	0.947	0.971	0.971	0.969	0.968	0.959	0.972	0.972	0.975	0.965
	G	0.956	0.975	0.974	0.971	0.969	0.959	0.971	0.972	0.975	0.969
	B	0.959	0.973	0.969	0.965	0.962	0.947	0.959	0.960	0.965	0.965
sCC	R	0.513	0.971	0.987	0.991	0.993	0.997	0.988	0.997	0.995	0.997
	G	0.500	0.976	0.990	0.994	0.995	0.998	0.989	0.997	0.995	0.997
	B	0.458	0.977	0.990	0.993	0.994	0.996	0.990	0.997	0.994	0.995
RASE(%)		25.86	20.39	20.91	21.63	22.20	25.29	23.23	21.82	20.45	22.40
ERGAS		6.43	5.09	5.24	5.43	5.57	6.36	5.87	5.52	5.16	5.60
Q4 ₃₂		0.974	0.987	0.987	0.986	0.985	0.980	0.976	0.981	0.984	0.983

TABLE II
LANDSAT ETM+ IMAGE FUSION RESULTS

		Initial	$t = 2.0$	$t = 3.0$	$t = 4.0$	$t = 5.0$	IHS	udWA	udWS	udGA	udRWM
Bias(%) (ideal value:0)	R	0.024	0.223	0.306	0.347	0.372	0.471	1.054	0.447	0.717	0.004
	G	0.212	0.435	0.509	0.547	0.569	0.658	1.182	0.590	0.879	0.224
	B	0.207	0.455	0.538	0.579	0.604	0.703	1.286	0.698	0.949	0.208
SD(%) (ideal value:0)	R	2.558	1.982	3.164	3.937	4.446	6.742	4.592	4.033	3.416	3.574
	G	2.030	1.333	2.621	3.434	3.960	6.260	4.517	2.603	3.087	1.956
	B	0.659	0.153	1.648	2.684	3.335	6.088	4.801	2.925	2.906	0.103
CC (ideal value:1)	R	0.972	0.975	0.972	0.969	0.968	0.960	0.965	0.962	0.968	0.965
	G	0.978	0.985	0.982	0.980	0.978	0.972	0.970	0.976	0.975	0.978
	B	0.969	0.970	0.961	0.955	0.951	0.935	0.933	0.941	0.944	0.963
sCC	R	0.601	0.950	0.975	0.982	0.985	0.992	0.978	0.996	0.987	0.990
	G	0.653	0.972	0.988	0.993	0.994	0.998	0.989	0.998	0.996	0.994
	B	0.610	0.975	0.988	0.991	0.992	0.993	0.988	0.996	0.992	0.989
RASE(%)		1.87	1.29	2.70	3.72	4.38	7.28	5.62	3.31	3.68	1.75
ERGAS		0.96	0.72	1.29	1.71	1.98	3.19	2.39	1.64	1.62	1.17
Q4 ₃₂		0.995	0.997	0.996	0.996	0.995	0.994	0.989	0.995	0.994	0.996

TABLE III
OBJECTIVE PERFORMANCE EVALUATION FOR IKONOS IMAGE FUSION

IFPM		$t = 2.0$	$t = 3.0$	$t = 4.0$	$t = 5.0$	IHS	udWA	udWS	udGA	udRWM
Source image	Fused image									
D(R)	F(R)	0.7860	0.7808	0.7788	0.7776	0.7747	0.7760	0.7770	0.7771	0.7839
D(G)	F(G)	0.7797	0.7747	0.7728	0.7717	0.7696	0.7703	0.7710	0.7711	0.7785
D(B)	F(B)	0.7742	0.7695	0.7677	0.7667	0.7639	0.7656	0.7662	0.7666	0.7744
Source image	Fused image									
PAN	F(R)	0.7773	0.7812	0.7832	0.7844	0.7878	0.7796	0.7810	0.7806	0.7757
PAN	F(G)	0.7763	0.7806	0.7826	0.7838	0.7879	0.7750	0.7752	0.7746	0.7722
PAN	F(B)	0.7715	0.7751	0.7766	0.7773	0.7797	0.7701	0.7703	0.7696	0.7676

In Table I, the values of the SD and CC of the proposed method with $t = 4.0$ are almost the same as the corresponding average values of the wavelet-based methods, even though the values of the bias of the proposed method are greater than those of the wavelet-based methods. In Table II, the values of the bias, SD, and CC of the proposed method with $t = 4.0$ are similar to the values of those of the wavelet-based methods. This re-

sult shows that the spectral quality of the fused images obtained by the proposed method with an appropriate tradeoff parameter could be as good as the spectral quality of the images obtained from the wavelet-based methods.

2) *RASE and the ERGAS*: To estimate the global spectral quality of the fused images, the index of the RASE is expressed as a percentage [3]–[5], [7], [8]. This percentage characterizes

TABLE IV
OBJECTIVE PERFORMANCE EVALUATION FOR LANDSAT ETM+ IMAGE FUSION

IFPM		$t = 2.0$	$t = 3.0$	$t = 4.0$	$t = 5.0$	IHS	udWA	udWS	udGA	udRWM
Source image	Fused image									
D(R)	F(R)	0.7640	0.7585	0.7562	0.7553	0.7512	0.7522	0.7501	0.7520	0.7524
D(G)	F(G)	0.7673	0.7622	0.7600	0.7591	0.7548	0.7515	0.7510	0.7516	0.7567
D(B)	F(B)	0.7473	0.7423	0.7402	0.7394	0.7363	0.7350	0.7335	0.7345	0.7419
Source image	Fused image									
PAN	F(R)	0.7034	0.7104	0.7135	0.7153	0.7206	0.7005	0.7114	0.7041	0.7059
PAN	F(G)	0.7232	0.7347	0.7401	0.7429	0.7492	0.7209	0.7595	0.7371	0.7351
PAN	F(B)	0.6965	0.7046	0.7076	0.7091	0.7122	0.6913	0.6969	0.6933	0.6879

the average performance of the method of image fusion in the spectral bands considered

$$\text{RASE} = \frac{100}{M} \sqrt{\frac{1}{N} \sum_{i=1}^N \text{RMSE}^2(B_i)} \quad (14)$$

where M is the mean radiance of the N spectral bands (B_i) of the original MS bands, and RMSE is the root mean square error computed in the following expression:

$$\text{RMSE}^2(B_i) = \text{bias}^2(B_i) + \text{SD}^2(B_i). \quad (15)$$

In the fusion, the index of the ERGAS (which means relative global dimensional synthesis error) is as follows:

$$\text{ERGAS} = 100 \frac{h}{l} \sqrt{\frac{1}{N} \sum_{i=1}^N \frac{\text{RMSE}^2(B_i)}{M_i^2}} \quad (16)$$

where h is the resolution of the high spatial resolution image, l is the resolution of the low spatial resolution image, and M_i is the mean radiance of each spectral band involved in the fusion. The lower the value of the RASE and ERGAS indexes, the higher the spectral quality of the fused images.

In Tables I and II, as the corresponding t increases from 2.0 to 5.0, the RASE and ERGAS values of the proposed method monotonically increase. The results, which indicate that the spectral quality of the fused images decreases when t increases, coincide with results of the bias, SD, and CC factors previously used for the experiments.

Moreover, in the case of the IKONOS and Landsat ETM+ image fusion, the RASE and ERGAS values of the wavelet-based image fusion methods are similar to the corresponding values of the proposed method for $t = 4.0$. This result means that simply by using an appropriate tradeoff parameter we can obtain good quality fused images that are similar to the images fused by wavelet-based image fusion.

3) *New Quality Index Q_4* : Although the score index of (16) encapsulates several measurements in a unique number, the index does not consider the CCs and fails to measure either the spectral distortion or the radiometric distortion [20]. Recently, Alparone *et al.* proposed a reliable image quality index, namely Q_4 , for MS images with four spectral bands [20]. The Q_4 index is a generalization of the Q index defined by Wang and Bovik and relies on the theory of quaternions, which are hypercomplex numbers, recently used for color image processing [22], [23]. See [24] to review the fundamentals of the theory of quaternions.

For the original MS images with four spectral bands, let a_1 , b_1 , c_1 , and d_1 denote the radiance values of a given image pixel in the four bands. For the fusion images with four spectral bands, let a_2 , b_2 , c_2 , and d_2 denote the radiance values of a given image pixel in the four bands. Let $z_1 = a_1 + ib_1 + jc_1 + kd_1$ and $z_2 = a_2 + ib_2 + jc_2 + kd_2$ respectively denote the four-band original MS image and the fusion product, both of which are expressed as quaternions. The new index is defined as

$$Q_4 = \frac{4 |\sigma_{z_1 z_2}| \cdot |\bar{z}_1| \cdot |\bar{z}_2|}{(\sigma_{z_1}^2 + \sigma_{z_2}^2) (|\bar{z}_1|^2 + |\bar{z}_2|^2)} \quad (17)$$

where $\sigma_{z_1 z_2}$ is the quaternion or hypercomplex covariance between z_1 and z_2 (see [25] for more details), σ_{z_1} and σ_{z_2} are the square roots of the variances of z_1 and z_2 , \bar{z}_1 and \bar{z}_2 are the expected values of z_1 and z_2 , respectively, and $|\cdot|$ is the modulus of \cdot . Equation (17) may be equivalently rewritten as a product of three terms as follows:

$$Q_4 = \frac{|\sigma_{z_1 z_2}|}{\sigma_{z_1} \cdot \sigma_{z_2}} \cdot \frac{2\sigma_{z_1} \cdot \sigma_{z_2}}{\sigma_{z_1}^2 + \sigma_{z_2}^2} \cdot \frac{2|\bar{z}_1| \cdot |\bar{z}_2|}{|\bar{z}_1|^2 + |\bar{z}_2|^2}. \quad (18)$$

The first term, which is the modulus of the hypercomplex CC between z_1 and z_2 , is sensitive both to the loss of correlation and to the spectral distortion between the two MS datasets. The second term measures the changes in the contrast, and the third term simultaneously measures the mean bias on all bands.

The ensemble expectations were calculated as averages on $N \times N$ blocks. Hence, Q_4 also depends on N and is denoted as Q_{4N} . Eventually, Q_{4N} was averaged over the entire image to yield the global score index. Because all the fusion methods yielded rather steady plots for $N > 16$ in [20], Q_4 with $N = 32$ was calculated and averaged on the entire image. As with color images, when there are three components, the real part of a quaternion is usually set to zero [23].

From the definition of Q_4 , Q_4 takes real values in the interval (0, 1), where 1 is the best value. Furthermore, the best value can be attained if and only if the fusion product is identical to the original MS dataset. The closer the value of the Q_{4N} index to 1, the higher the spectral quality of the fusion product.

In Tables I and II, whenever the corresponding t enlarges from 2.0 to 5.0, the values Q_{432} of the proposed method monotonically decrease. This result means that the spectral quality of fusion product decreases when t increases, and that the factor used for the experiment is also appropriate.

In addition, the Q_{432} values of the proposed method with $t = 5.0$ are similar to those of the wavelet-based methods. This result also shows that the spectral quality of the fused images

obtained from the proposed method with an appropriate tradeoff parameter could be as good as the spectral quality of the images obtained from the wavelet-based methods.

4) *IFPM*: To evaluate the amount of information transferred from the source image and the final fused image, we used the IFPM proposed by Tsagaris *et al.* [21]. The IFPM, which is based on information theory, is defined as follows:

$$\text{IFPM} = \frac{\text{CI}}{\text{H}(X)} \quad (19)$$

where $\text{CI} = \text{H}(X) - \text{H}(X|Y)$ for the final fused image Y and the source image X ; $\text{H}(X)$ is the entropy of the source image X ; and $\text{H}(X|Y)$ is the conditional entropy of the source image X when given the final fused image Y . The term CI represents the amount of common information between the source image and the final fused image, whereas the entropy $\text{H}(X)$ represents the total amount of information for the source image [21].

Therefore, the IFPM takes real values in the interval $(0, 1)$, where 0 corresponds to the total lack of common information between the source and the fused image and 1 corresponds to an extremely effective fusion process that transfers all the information from the source image to the fused image.

In Tables III and IV, when the source images are the spatially degraded MS images or the initial MS images, the IFPM values of the proposed method monotonically decrease when the corresponding t enlarges from 2.0 to 5.0. This result means that the amount of spectral information transferred from the initial MS images to the final fused images decreases when t increases. That is, the spectral resolution of the images fused by the proposed method decreases when t increases.

In contrast, when the source images are the Pan image, the IFPM values of the proposed method monotonically increase when the corresponding t enlarges from 2.0 to 5.0, thereby indicating that the amount of spatial information transferred from the Pan image to the final fused images increase when t increases. That is, the spatial resolution of the images fused by the proposed method increases when t increases. This phenomenon therefore supports the notion that the parameter t can be used to easily control the tradeoff between the spatial and spectral resolution of the image to be fused.

Additionally, the IFPM values of the proposed method with $t = 4.0$ and $t = 5.0$ are similar to the IFPM values of the wavelet-based methods. This result also coincides with the predictions for the experiments.

5) *Spatial Quality Measurement Proposed by Zhou et al.*: To evaluate the detailed spatial information, a procedure proposed by Zhou *et al.* [6] was used. In this procedure, the Pan was filtered and images fused with a Laplacian filter as follows:

$$\begin{bmatrix} -1 & -1 & -1 \\ -1 & 8 & -1 \\ -1 & -1 & -1 \end{bmatrix}. \quad (20)$$

The high correlation coefficients between the fused filtered image and the Pan-filtered image (sCC) indicate that most of the spatial information of the Pan image was incorporated during the merging process.

The sCC has the same definition as the CC. In Tables I and II, the sCC of the proposed method monotonically increases when the corresponding t enlarges from 2.0 to 5.0. This result

means that the spatial resolutions of images fused by the proposed method increase whenever t enlarges.

In summary, when the corresponding t enlarges from 2.0 to 5.0, the spatial resolutions of the images fused by the proposed method monotonically increase, whereas the spectral resolutions decrease. These results confirm that the tradeoff parameter t can be used to easily control the tradeoff between the spatial and spectral resolutions of the image to be fused. The results also show that the spectral and spatial quality of the fused images obtained by the proposed method with an appropriate tradeoff parameter could be as good as the spectral and spatial quality of the images obtained from the wavelet-based methods.

B. Visual Analysis

Figs. 2 and 3 show the results of the visual fusion. As with the quantitative analysis, these results show that, depending on the enlarger of the tradeoff parameter t , the spatial resolution of the images fused by the proposed method monotonically increases whereas the spectral resolution decreases.

For visual analysis, Fig. 2(c) and (d) and Fig. 3(c) and (d) fused by the proposed method with $t = 2.0$ and $t = 3.0$ are slightly blurrier than the images fused by the wavelet-based methods. This difference occurs because the wavelet transform represents edges well, thereby producing clearer images. As a result, to obtain shaper fused images, a tradeoff parameter of 4.0 is well suited for the IKONOS image fusion. Furthermore, a tradeoff parameter of 5.0 is well suited for Landsat ETM+ image fusion.

However, an explicit algorithm for choosing an appropriate tradeoff parameter that corresponds to a given application was not given. This drawback presupposes considerable trial and error in choosing an appropriate tradeoff parameter. However, after choosing a tradeoff parameter that corresponds to a given application, the parameter can be used continuously. For example, according to the experimental results in this work, 4.0 is a well-suited tradeoff parameter for the IKONOS image fusion and 5.0 is a well-suited tradeoff parameter for the Landsat ETM+ image fusion.

C. Color-Enhanced Fusion Result

Fig. 4 shows the color-enhanced results of fusion by the proposed method on two different regions of IKONOS. The top image of Fig. 4 shows a golf course with wide regions of vegetation. The bottom image of Fig. 4 shows an urban zone with buildings, roads, and a river. In Fig. 4, the vegetation zones of the original MS image are much darker because the vegetation appears to have relatively low reflectance in RGB bands. To overcome this problem and to obtain a color-enhanced image, three different tradeoff parameters were used for each MS image, and the parameters were based on basic knowledge of the IKONOS spectral response (Fig. 1). To separate the green and blue bands that overlap substantially, t was used for G, which was greater than t for B, in (11). Furthermore, because the RGB bands were expected to fall just within the spectral range of the Pan band, a t value that was larger than 2.0 for all RGB bands was used. The color-enhanced fusion results of Fig. 4 were obtained just by applying the three different tradeoff parameters of

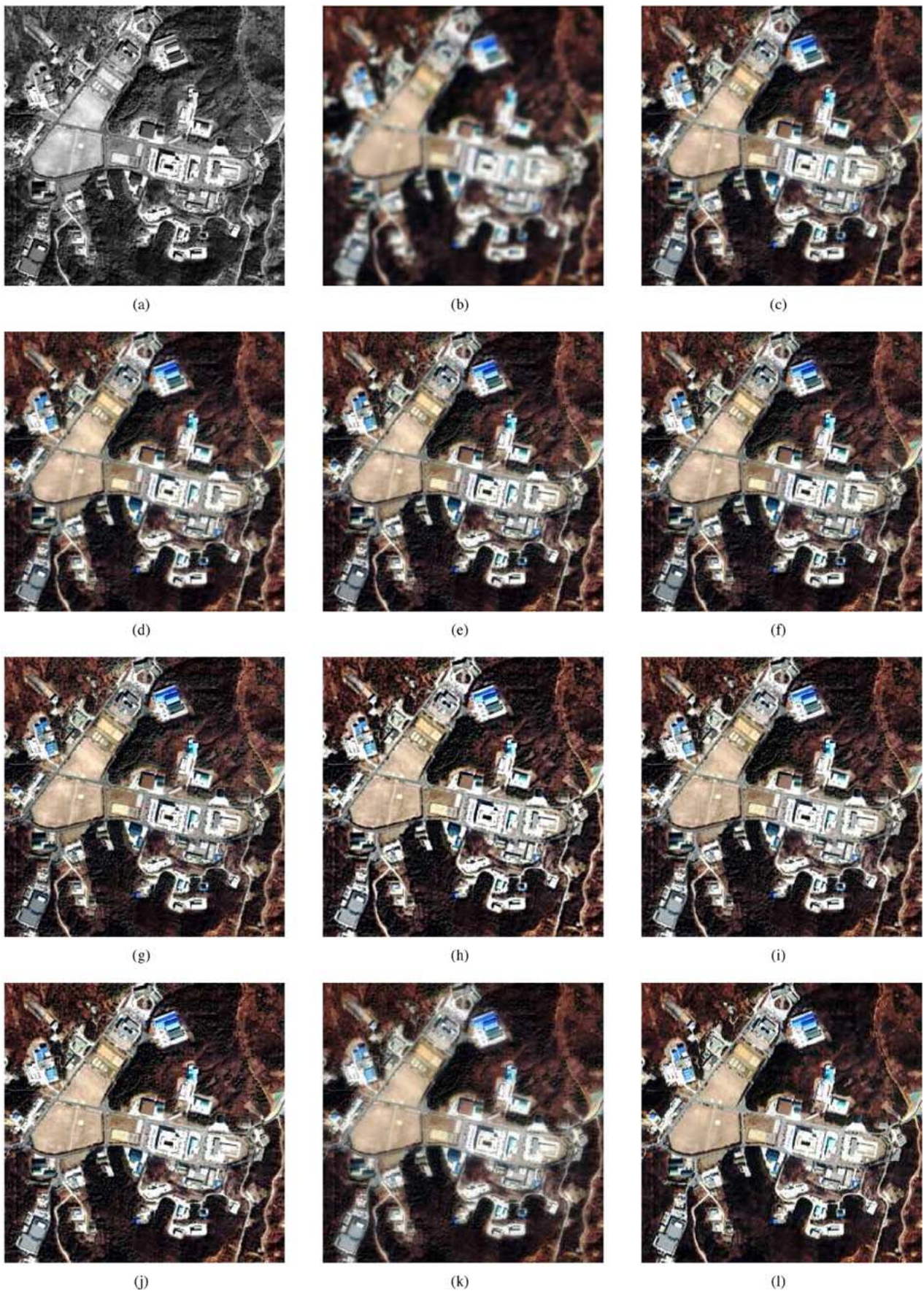


Fig. 2. (a) IKONOS Pan image. (b) Degraded color image. (c) Result image for $t = 2.0$. (d) Result image for $t = 3.0$. (e) Result image for $t = 4.0$. (f) Result image for $t = 5.0$. (g) Fused by IHS (h) Fused by udWA. (i) Fused by udWS. (j) Fused by udGA. (k) Fused by udRWM. (l) Original IKONOS color image.

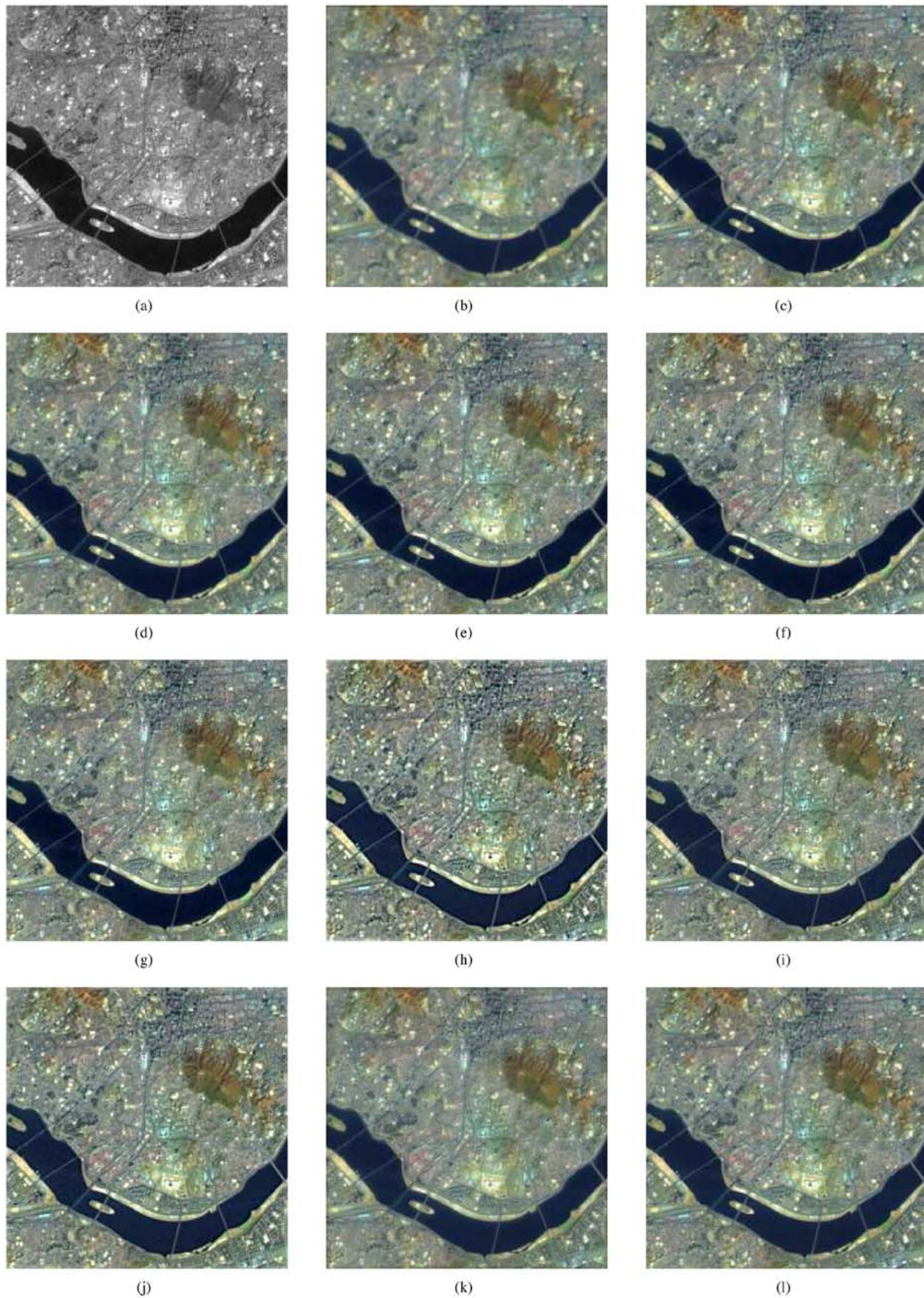


Fig. 3. (a) Landsat ETM+ Pan image. (b) Degraded color image. (c) Result image for $t = 2.0$. (d) Result image for $t = 3.0$. (e) Result image for $t = 4.0$. (f) Result image for $t = 5.0$. (g) Fused by IHS. (h) Fused by udWA. (i) Fused by udWS. (j) Fused by udGA. (k) Fused by udRWM. (l) Original Landsat ETM+ color image.



Fig. 4. IKONOS color image of Daejeon, Korea, with the resampled (reduced) original MS color images (top left); (reduced) color-enhanced results of fusion by the proposed method (bottom left); and (slightly reduced) color-enhanced fusion results (right).

$t = 2.5$ for R, $t = 3.5$ for G, and $t = 2.0$ for B. Finally, with the aid of appropriate tradeoff parameters, the fused image can be color-enhanced or modified according to a user's specifications.

IV. CONCLUSION

We have presented a new approach for image fusion based on the fast IHS method. The proposed method is a fast, convenient approach to image fusion in which the parameter t is

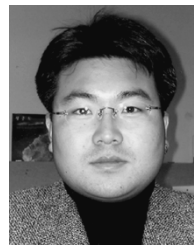
used to appropriately control a tradeoff between the spatial and spectral resolution of the image to be fused. To validate this new approach, the approach was used to merge IKONOS images, Landsat ETM+ Pan images and MS images. Moreover, to analyze the spatial and spectral quality of the resulting images, the following eight factors were used: bias, SD, CC, RASE, ERGAS, Q_4 , IFPM, and sCC. The results were then compared with the quality of images fused by wavelet-based fusion methods. The final results show that, with an appropriate tradeoff parameter, the proposed method provides satisfactory results, both visually and quantitatively.

ACKNOWLEDGMENT

The author would like to express their sincere gratitude to the anonymous referees for pointing out several typos and for some very helpful comments, and thank Korea Institute of Geoscience and Mineral Resources and Korea Aerospace Research Institute for providing the IKONOS images for this research.

REFERENCES

- [1] C. K. Munechika, J. S. Warnick, C. Salvaggio, and J. R. Schott, "Resolution enhancement of multispectral image data to improve classification accuracy," *Photogramm. Eng. Remote Sens.*, vol. 59, no. 1, pp. 67–72, 1993.
- [2] Y. Zhang, "Understanding image fusion," *Photogramm. Eng. Remote Sens.*, vol. 70, no. 6, pp. 653–760, 2004.
- [3] L. Wald, T. Ranchin, and M. Mangolini, "Fusion of satellite images of different spatial resolution: Assessing the quality of resulting images," *Photogramm. Eng. Remote Sens.*, vol. 63, no. 6, pp. 691–699, 1997.
- [4] T. Ranchin and L. Wald, "Fusion of high spatial and spectral resolution images: the arsis concept and its implementation," *Photogramm. Eng. Remote Sens.*, vol. 66, pp. 49–61, 2000.
- [5] T. Ranchin, B. Aiazzi, L. Alparone, S. Baronti, and L. Wald, "Image fusion—the ARSIS concept and some successful implementation schemes," *ISPRS J. Photogramm. Remote Sens.*, vol. 58, pp. 4–18, 2003.
- [6] J. Zhou, D. L. Civco, and J. A. Silander, "A wavelet transform method to merge Landsat TM and SPOT panchromatic data," *Int. J. Remote Sens.*, vol. 19, no. 4, pp. 743–757, 1998.
- [7] M. González-Audícana, J. L. Saleta, R. G. Catalán, and R. García, "Fusion of multispectral and panchromatic images using improved IHS and PCA mergers based on wavelet decomposition," *IEEE Trans. Geosci. Remote Sens.*, vol. 42, no. 6, pp. 1291–1299, Jun. 2004.
- [8] M. Choi, R. Y. Kim, M.-Y. Nam, and H. O. Kim, "Fusion of multispectral and panchromatic satellite images using the curvelet transform," *IEEE Geosci. Remote Sens. Lett.*, vol. 2, no. 2, pp. 136–140, Feb. 2005.
- [9] B. Aiazzi, L. Alparone, S. Baronti, and A. Garzelli, "Context-driven fusion of high spatial and spectral resolution data based on oversampled multiresolution analysis," *IEEE Trans. Geosci. Remote Sens.*, vol. 40, no. 10, pp. 2300–2312, Oct. 2002.
- [10] Y. Chibani and A. Houacine, "The joint use of IHS transform and redundant wavelet decomposition for fusing multispectral and panchromatic images," *Int. J. Remote Sens.*, vol. 23, no. 18, pp. 3821–3833, 2002.
- [11] Y. Chibani and A. Houacine, "Redundant versus orthogonal wavelet decomposition for multisensor image fusion," *Pattern Recognit.*, vol. 36, pp. 879–887, 2003.
- [12] C. Pohl and J. L. Van Genderen, "Multisensor image fusion in remote sensing: concepts, methods and applications," *Int. J. Remote Sens.*, vol. 19, no. 5, pp. 823–854, 1998.
- [13] J. Núñez, X. Otazu, O. Fors, A. Prades, V. Palà, and R. Arbiol, "Multiresolution-based image fusion with additive wavelet decomposition," *IEEE Trans. Geosci. Remote Sens.*, vol. 37, no. 3, pp. 1204–1211, Mar. 1999.
- [14] J. G. Liu, "Smoothing filter-based intensity modulation: A spectral preserve image fusion technique for improving spatial details," *Int. J. Remote Sens.*, vol. 21, pp. 3461–3472, 2000.
- [15] —, "Evaluation of Landsat-7 ETM+ panchromatic band for image fusion with multispectral bands," *Natural Resources Res.*, vol. 9, no. 4, pp. 269–276, 2000.
- [16] W. Shi, C. Zhu, C. Zhu, and X. Yang, "Multi-band wavelet for fusing SPOT panchromatic and multispectral images," *Photogramm. Eng. Remote Sens.*, vol. 69, no. 5, pp. 513–520, 2003.
- [17] T.-M. Tu, P. S. Huang, C.-L. Hung, and C.-P. Chang, "A fast intensity-hue-saturation fusion technique with spectral adjustment for IKONOS imagery," *IEEE Geosci. Remote Sens. Lett.*, vol. 1, no. 4, pp. 309–312, Apr. 2004.
- [18] T.-M. Tu, S.-C. Su, H.-C. Shyn, and P. S. Huang, "A new look at IHS-like image fusion methods," *Inform. Fusion*, vol. 2, no. 3, pp. 177–186, 2001.
- [19] P. Dutilleul, "An implementation of the "algorithme à trous" to compute the wavelet transform," in *Wavelets: Time-Frequency Methods and Phase Space*, J. M. Combes, A. Grossman, and P. Tchamitchian, Eds. Berlin, Germany: Springer-Verlag, 1989, pp. 298–304.
- [20] L. Alparone, S. Baronti, A. Garzelli, and F. Nencini, "A global quality measurement of pan-sharpened multispectral imagery," *IEEE Geosci. Remote Sens. Lett.*, vol. 1, no. 4, pp. 313–317, Apr. 2004.
- [21] V. Tsagaris and V. Anastassopoulos, "An information measure for assessing pixel-level fusion methods," *Proc. SPIE*, vol. 5573, pp. 64–71, 2004.
- [22] Z. Wang and A. C. Bovik, "A universal image quality index," *IEEE Signal Process. Lett.*, vol. 9, no. 1, pp. 81–84, Jan. 2002.
- [23] S. J. Sangwine and T. A. Ell, "Color image filters based on hypercomplex convolution," *Proc. Inst. Elect. Eng.—Vision, Image, Signal Process.*, vol. 147, no. 2, pp. 89–93, 2000.
- [24] I. L. Kantor and A. S. Solodnikov, *Hypercomplex Numbers, An Elementary Introduction to Algebras*. New York: Springer-Verlag, 1989.
- [25] C. E. Moxey, S. J. Sangwine, and T. A. Ell, "Hypercomplex correlation techniques for vector images," *IEEE Trans. Signal Process.*, vol. 51, no. 7, pp. 1941–1953, Jul. 2003.



Myungjin Choi (S'04) received the B.S. degree in mathematics in 2000 from Soongsil University, Korea, and the M.S. degree in applied mathematics in 2002 from the Korea Advanced Institute of Science and Technology (KAIST), Daejeon, where he is currently pursuing the Ph.D. degree.

Since 2002, he has been a Researcher with the Satellite Technology Research Center, KAIST. His current research activity involves multiresolution analysis, frames, multisensor data fusion, and image processing.